Article

J. Biol. Regul. Homeost. Agents. 2024; 38(6): 4851–4861
https://doi.org/10.23812/j.biol.regul.homeost.agents.20243806.388

Gambogenic Acid Induces Apoptosis and Protective Autophagy in Human Osteosarcoma Cells

Rui Zhang[1,†], Tao Liu[1,†], Peng Qiu[1], Xiaoyan Wang[1], Bene Qian[1], Xianqing Sun[1], Xiang Li[1,*]

[1]Department of Orthopedic Trauma, The First People's Hospital of Qujing, 655000 Qujing, Yunnan, China
*Correspondence: 13987440066@163.com (Xiang Li)
[†]These authors contributed equally.
Submitted: 2 January 2024 Revised: 5 February 2024 Accepted: 5 March 2024 Published: 1 June 2024

Background: The impact of Gambogenic acid (GNA), a bioactive component derived from Gamboge, on osteosarcoma (OS) has not been properly investigated. However, whether GNA could induce autophagy in osteosarcoma cells and its role in inducing autophagy of osteosarcoma remains unclear. Therefore, this study aimed to elucidate apoptosis and autophagy in GNA-treated-143B cells and to explore the association between apoptosis and autophagy in these cells after treatment.

Methods: The inhibitory effect of GNA on 143B cells was assessed using Cell Counting Kit-8 (CCK-8) assay. Hoechst staining and flow cytometric analysis were used to examine the apoptosis rate, and Ad-GFP-LC3B transfection was employed to evaluate autophagy in treated cells. Intracellular reactive oxygen species (ROS) level and mitochondrial membrane potential were determined through 2′,7′-Dichlorodihydrofluorescein diacetate (DCFH-DA) and 5,5′,6,6′-tetrachloro-1,1′,3,3′-tetramethylbenzimidazolylcarbocyanine iodide (JC-1) staining, respectively. Additionally, Western blot analysis was utilized to assess the expression of apoptosis-related proteins, autophagy, c-Jun N-terminal kinase (JNK) signaling pathway, and mitochondrial apoptosis pathway.

Results: The GNA treatment significantly inhibited 143B cell viability and Colony formation ($p < 0.05$). We observed the involvement of mitochondrial pathways in GNA-induced cell apoptosis ($p < 0.05$). Furthermore, GNA treatment induced autophagy, which was suppressed by reactive oxygen species (ROS) scavenger and JNK inhibitor ($p < 0.05$). Thus, the ROS scavenger hindered JNK phosphorylation ($p < 0.05$). Inhibition of autophagy by knockdown of AGT5 enhanced both apoptosis rate and cytotoxicity of 143B cells following GNA treatment ($p < 0.05$).

Conclusions: GNA induced apoptosis and autophagy in 143B cells, with apoptosis being associated with the mitochondrial pathway and autophagy being regulated by the ROS-JNK signaling pathway. Additionally, autophagy played a cell-protective role against apoptosis.

Keywords: osteosarcoma; gambogic acid; apoptosis; autophagy

Background

Osteosarcoma (OS) is the prevailing malignant tumor originating from the bone, primarily affecting teenagers and children, leading to significant disability and mortality rates [1,2]. The treatment of OS primarily involves surgery, supplemented by neoadjuvant chemotherapy [3–6]. Despite the improvement in the clinical outcome of early non-metastatic OS patients through high-dose combination chemotherapy, the adverse effects linked to commonly utilized chemotherapy medications like doxorubicin, cisplatin, ifosfamide, and methotrexate need considerable attention. Additionally, increased drug dosage may lead to reduced sensitivity [5,7,8]. Consequently, there is a crucial need to explore more effective alternative treatment strategies against OS.

Gambogenic acid (GNA) is a major bioactive component derived from gamboge [9]. Recently, GNA has been found to have significant inhibitory effects against various cancer types, including melanoma, bladder cancer, colorectal cancer, and nasopharyngeal carcinoma, causing comparatively minimal toxicity [10–13]. As a result, GNA holds potential as a promising candidate for cancer therapy.

Autophagy, the process of breaking down proteins and organelles to generate energy and remove damaged organelles, plays a pivotal role in maintaining cellular balance [14,15]. However, the impact of autophagy on the development, progression, and treatment of tumors is like a double-edged sword. Moreover, depending on factors such as cancer type, stage, and intervention strategies, autophagy can either suppress or promote the initiation of tumors. Although the anti-OS effects of GNA have been studied, there remains controversy regarding its impact on autophagy in tumor cells [16,17]. Wang *et al*. [18] found that GNA can inhibit basal autophagy levels in drug-resistant liver cancer cells, thereby increasing their sensitivity to doxorubicin.

Journal of
BIOLOGICAL REGULATORS
and Homeostatic Agents

Conversely, Wu *et al*. [19] indicated that GNA might induce cytoprotective autophagy in prostate cancer cells.

Therefore, we aimed to elucidate whether GNA could induce autophagy in OS cells and to explore the combined inhibitory effect of GNA and autophagy inhibition in OS treatment. Our findings demonstrated that GNA induced both apoptosis and autophagy in OS cells, regulated through the involvement of the mitochondrial pathway and reactive oxygen species-Jun N-terminal kinase (ROS-JNK) pathway. Furthermore, GNA-induced autophagy in OS cells exhibited a cytoprotective effect.

Methods

Reagents

GNA was obtained from MCE (HY-N5024, MCE, Shanghai, China) and was dissolved in DMSO (ST038, Beyotime, Shanghai, China) to form a 20 mM stock solution. Other research materials, including N-acetyl-l-cysteine (NAC) (A9165), 2′,7′-Dichlorodihydrofluorescein diacetate (DCFH-DA) (D6883), and SP600125 (420119) were purchased from Sigma-Aldrich (St-Louis, MO, USA). However, the 5,5′,6,6′-tetrachloro-1,1′,3,3′-tetramethylbenzimidazolylcarbocyanine iodide (JC-1) (M8650) and Cell Counting Kit-8 (CCK-8) (CA1210) were purchased from Solarbio (Beijing, China). The Hoechst 33258 (C1017) was obtained from Beyotime (Shanghai, China).

Cell Culture

The culture of 143B cells (KGG3314-1, KeyGEN BioTECH, Nanjing, China) was established in Medium with High Glucose (DMEM) (PM150210, Procell, Wuhan, China) containing 10% fetal bovine serum (164210, Procell, Wuhan, China), 100 U/mL penicillin (PB180120, Procell, Wuhan, China), and 100 mg/mL streptomycin (PB180120, Procell, Wuhan, China), and subsequently incubated in a humidified incubator at 37 °C in the presence of 5% CO_2. The cells were authenticated using STR profiling and examined for contamination utilizing mycoplasma testing, and no cross-contamination between cells and no mycoplasma contamination were found.

According to the experiment purpose, the cells were divided into the following groups: the control group (the cells without any treatment), the GNA group (the cells treated with 1.35 μM GNA for 24 hours), the NAC group (the cells treated with 10 mM for 1 hour), the SP600125 group (the cells treated with 10 μM SP600125 for 1 hour), GNA + NAC group (the GNA-treated cells were exposed to NAC for 1 hour), and GNA + SP600125 group (the GNA-treated cells were exposed and SP600125 for 1 hour).

Cell Viability Assay

The 143B cells were seeded in 96-well plates and subsequently incubated for 24 hours. After achieving the required confluence, the cells were subjected to various treatments based on their assigned groups and were incubated for another 24 hours. After this, 10 μL of CCK-8 reagent was added to each well followed by incubation. Finally, the absorbance at 450 nm was evaluated utilizing a microplate reader (Infinite® 200 Pro, TECAN, Männedorf, Switzerland). The viability of cells was assessed using the following formula: Cell viability (%) = average optical density (OD) in the study group/average OD in the control group × 100%. Furthermore, the inhibitory concentration $(IC)_{25}$, IC_{50}, and IC_{75} concentrations of GNA against 143B cells were selected as the treatment conditions for subsequent experiments.

Apoptosis Observed by Hoechst Staining

The cells were exposed to GNA for 24 hours. Following incubation, the culture medium was removed and the cells underwent three consecutive Phosphate-Buffered Saline (PBS) washes. After this, 200 μL of Hoechst 33258 reagent (10 μg/mL) was introduced into each well and incubated for 5 minutes. After another round of PBS wash, the cells were observed using a fluorescence microscope (BX51, Olympus, Tokyo, Japan).

Colony Formation Assay

The cells were cultured in 6-well plates at a density of 1000 cells per well. The cells were then exposed to GNA for 24 hours followed by incubation for two weeks. After this, the cells were fixed with paraformaldehyde (P0099, Beyotime, Shanghai, China) and subsequently underwent staining with crystal violet (C0121, Beyotime, Shanghai, China). Finally, cells were examined using a microscope and the colonies were counted using Image-Pro Plus (version 6.0.0.260, Media Cybernetics, Rockville, MD, USA).

SiRNA Transfection

SiRNA targeting autophagy related gene 5 (*ATG5*) was procured from APExBIO (Shanghai, China). The siRNA sequences were as follows: small interfering RNA targeting *ATG5* (si*ATG5*): 5′-CCUGAACAGAAUCAUCCUUAA-3′; small interfering RNA targeting negative control (siNC): 5′-UUCUCCGAACGUGUCACGUTT-3′. The cells were transfected with si*RNA* utilizing Lipofectamine 8000 reagent (C0533, Beyotime, Shanghai, China) following the manufacturer's guidelines. For transfection purposes, 32 μL of Lipofectamine 8000 and 800 pmol of siRNA were mixed into 1 mL serum-free DMEM. Following a 20-minute incubation at ambient temperature, the mixture was introduced into the cell culture dish with a cell fusion rate of 80%. After transfection for 24 hours, the cells underwent specified treatment. Finally, 2 days after transfection knockdown efficiency was determined employing Western blot analysis.

Table 1. A list of antibodies used in Western blot analysis.

Target	Product code	Host	Source	Dilution	Secondary antibody
Pro-Caspase 3	R22842	Rabbit	Zenbio, Chengdu, China	1000	Anti-rabbit
Cleaved-Caspase 3	341034	Rabbit	Zenbio, Chengdu, China	1000	Anti-rabbit
Cleaved-PARP1	380374	Rabbit	Zenbio, Chengdu, China	1000	Anti-rabbit
Cytochrome C	R22867	Rabbit	Zenbio, Chengdu, China	1000	Anti-rabbit
Bax	R22708	Rabbit	Zenbio, Chengdu, China	1000	Anti-rabbit
Bcl-2	R23309	Rabbit	Zenbio, Chengdu, China	1000	Anti-rabbit
LC3	R381544	Rabbit	Zenbio, Chengdu, China	1000	Anti-rabbit
Beclin-1	381896	Rabbit	Zenbio, Chengdu, China	1000	Anti-rabbit
p62	R25788	Rabbit	Zenbio, Chengdu, China	1000	Anti-rabbit
T-JNK	R22866	Rabbit	Zenbio, Chengdu, China	1000	Anti-rabbit
P-JNK	R381100	Rabbit	Zenbio, Chengdu, China	1000	Anti-rabbit
ATG5	R23497	Rabbit	Zenbio, Chengdu, China	1000	Anti-rabbit
GAPDH	200306	mouse	Zenbio, Chengdu, China	1000	Anti-mouse
Goat Anti-Mouse IgG	511103	Goat	Zenbio, Chengdu, China	5000	/
Goat Anti-Rabbit IgG	511203	Goat	Zenbio, Chengdu, China	5000	/

JNK, Jun N-terminal kinase; T, total; P, phosphorylated; PARP, poly ADP-ribose polymerase; Bax, BCL2-associated X protein; Bcl-2, Apoptosis regulator Bcl-2; LC3, microtubule-associated protein 1 light chain 3; ATG, autophagy related gene; GAPDH, glyceraldehyde-3-phosphate dehydrogenase.

Autophagic Autophagosome Observed through Ad-GFP-LC3B Transfection

The cells were transfected with Ad-GFP-LC3B (C3006, Beyotime, Shanghai, China) following the manufacturer's instructions. The culture medium was refreshed, and the cells were treated with GNA for 12 hours. Finally, cell nuclei were stained with DAPI, and observed using a fluorescence microscope (BX51, Olympus, Tokyo, Japan).

Assessment of Intracellular ROS through DCFH-DA Staining

The cells were seeded in 6-well plates followed by a 12-hour exposure to GNA. After this, 10 μM DCFH-DA staining solution was added to each well and incubated for 20 minutes. After a thorough washing step, the fluorescence of intracellular ROS was observed using a fluorescence microscope (BX51, Olympus, Tokyo, Japan) and analyzed through Image-Pro Plus (version 6.0.0.260, Media Cybernetics, Rockville, MD, USA).

Evaluation of Mitochondrial Membrane Potential (Mt$\Delta\psi$) Using JC-1 Staining

Following a 12-hour exposure to GNA, 1 mL of JC-1 solution was introduced into each well followed by incubation for 20 minutes. Subsequently, the cells were washed with staining buffer and observed utilizing a fluorescence microscope (BX51, Olympus, Tokyo, Japan) as well as collected for flow cytometry assay.

Flow Cytometry

After the indicated treatments, the cells underwent trypsin digestion followed by centrifugation. In the next step, the cells were resuspended in 1× binding buffer provided in the Annexin V-Propidium iodide (PI) apoptosis detection kit (BB-4102, BestBio, Shanghai, China), and their concentration was adjusted to 1×10^6/mL. After this, 5 μL of Annexin V and 5 μL of PI solution were added into 400 μL of cell suspension followed by incubation at room temperature for 10 minutes in the dark. Finally, the apoptosis rate was assessed utilizing a flow cytometer (Navios 2L 8C, Beckman, Brea, CA, USA) and analyzed through the FlowJo V10 software (Ashland, Franklin, NJ, USA).

Western Blot

After treatments, the cells were harvested and underwent lysis in radioimmunoprecipitation assay buffer (P0013B, Beyotime Shanghai, China) containing protease (P1005, Beyotime, Shanghai, China) and phosphatase inhibitors (P1260, Solarbio, Beijing, China). The cells were placed on ice for 30 minutes and processed through ultrasonic cell lysis apparatus. Moreover, total proteins were collected through centrifugation. Furthermore, cytoplasmic proteins were extracted using a cell mitochondrial isolation kit (C3601, Beyotime, Shanghai, China) following the manufacturer's instruction. For cytoplasmic protein extraction, cells were resuspended in a mitochondrial separation reagent followed by homogenization and centrifugation. The resulting supernatant was collected, and the proteins were quantified employing a BCA protein quantification kit (P0010S, Beyotime, Shanghai, China). After this, the proteins were mixed with sodium dodecyl sulfate polyacrylamide gel electrophoresis (SDS-PAGE) loading buffer (P0015, Beyotime, Shanghai, China) and subsequently heated. In the next step, proteins were separated using SDS-PAGE and subsequently transferred onto PVDF membranes. The membranes were blocked with 5% skim

Journal of
BIOLOGICAL REGULATORS
and Homeostatic Agents

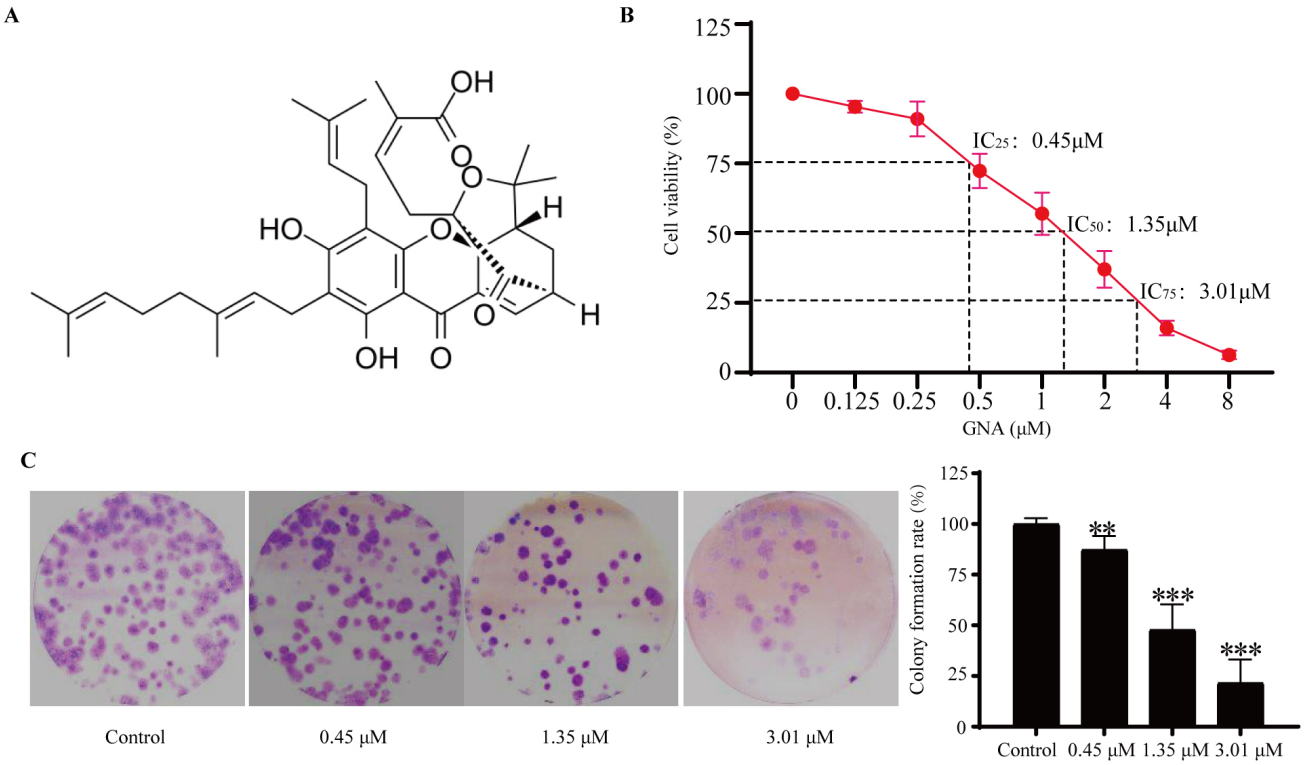

Fig. 1. GNA inhibited the viability and proliferation of 143B cell lines. (A) The chemical structure of GNA. (B) Cell viability of 143B cells following treatment with GNA at concentrations of 0, 0.125, 0.25, 0.5, 1, 2, 4 and 8 μM for 24 hours. (C) Colony formation assay. $^{**}p < 0.01$ vs. the control group (n = 3), $^{***}p < 0.001$ vs. the control group (n = 3). GNA, Gambogenic acid; IC, inhibitory concentration.

milk at room temperature for 2 hours. After this, the membranes underwent overnight incubation with corresponding primary antibodies at 4 °C (Table 1). The following day, the membranes were washed with TBST, and exposed to a horseradish peroxidase-labeled secondary antibody for 1 hour (Table 1). Following a thorough washing step, the immunoblots were developed using an ECL kit (17047, Zenbio, Chengdu, China) and a gel imaging system (Fusion FX, Vilber, Paris, France). Finally, the grayscale values of the protein bands were determined using Image J software (Version 1.51j8, National Institutes of Health, Bethesda, MD, USA). The β-actin was used as an internal control.

Statistical Analysis

Statistical analyses were performed using SPSS (Version 19, IBM, New York, NY, USA). Each experiment was independently replicated three times and data were presented as mean ± SD. The comparison of the two groups was conducted using a *t*-test, while one-way ANOVA was employed for multiple-group comparisons. However, S-N-K (Student-Newman-Keuls) was used for post hoc analysis. The statistical significance was indicated at a *p*-value of <0.05.

Results

GNA Exerted a Potential Anti-Proliferative Effect on OS 143B Cells

The chemical structure of GNA is shown in Fig. 1A. The CCK-8 assay revealed that following 24-hour exposure, the IC_{25}, IC_{50}, and IC_{75} concentrations of GNA against 143B were 0.45 μM, 1.35 μM, and 3.01 μM, respectively, and these concentrations were used for subsequent experiments (Fig. 1B). Furthermore, GNA significantly suppressed the colony formation capability of 143B cells ($p < 0.05$, Fig. 1C). These findings indicate a potential anti-proliferative effect of GNA on OS 143B cells.

GNA Treatment Induced Apoptosis in 143B Cells

To observe the morphological changes in 143B cells after treatment, we employed Hoechst 33258 for cell nucleus staining and examined the apoptotic alterations through a fluorescence microscope. Following 24 hours of GNA treatment, the chromatin density of 143B cells was enhanced, resulting in a bright blue appearance (Fig. 2A). Additionally, they exhibited the characteristic morphological alterations associated with apoptosis, such as nuclear shrinkage, compaction, and nuclear fragmentation. Nevertheless, the control group remained unchanged. Furthermore, Western blot revealed that GNA treatment signifi-

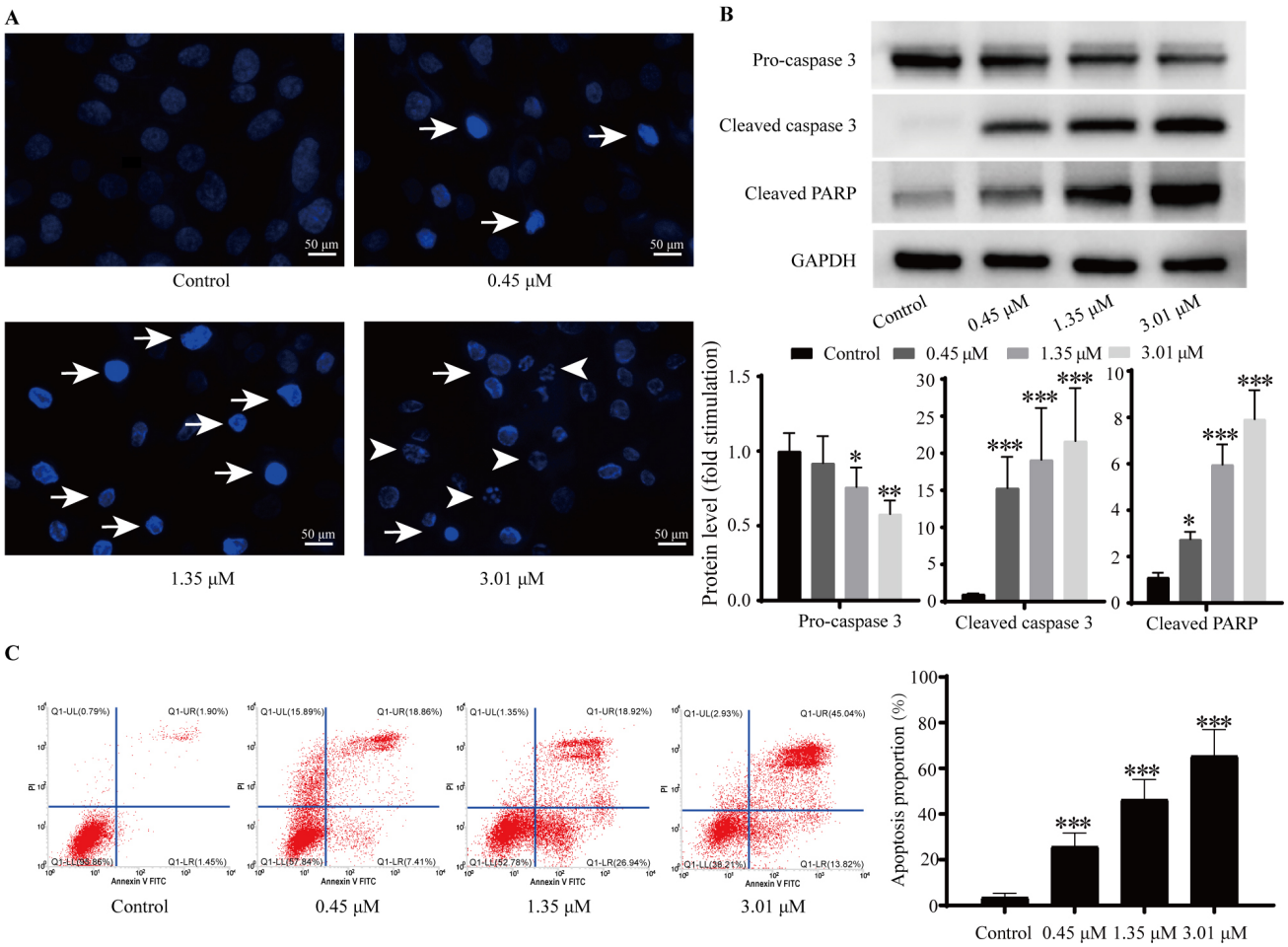

Fig. 2. GNA treatment induced apoptosis in 143B cells. (A) Hoechst 33258 staining of 143B cells. Arrowhead; nuclear shrinkage, compaction, and bright staining; Arrow: nuclear fragmentation. (B) Protein expression levels were assessed using Western blot. (C) The apoptosis ratio was assessed using flow cytometric analysis. $^{*}p < 0.05$ vs. the control group (n = 3), $^{**}p < 0.01$ vs. the control group (n = 3), $^{***}p < 0.001$ vs. the control group (n = 3).

cantly increased the expression levels of cleaved caspase-3 and cleaved poly ADP-ribose polymerase (PARP) ($p < 0.05$, Fig. 2B). Additionally, the flow cytometry assay showed a significantly higher level of apoptosis following 24 hours of GNA treatment ($p < 0.05$, Fig. 2C). These findings suggest that GNA treatment induced apoptosis in 143B cells.

GNA-Induced Apoptosis Involves the Mitochondrial Pathway

Since GNA has been recognized for the potential to harm the mitochondria of 143B cells [19,20]; thus, we inferred that apoptosis induced in these cells by GNA might be linked to the mitochondrial pathway. JC-1 serves as a fluorescent indicator to detect Mt$\Delta\psi$. Under homeostatic conditions, the Mt$\Delta\psi$ remains normal, leading JC-1 to aggregate and emit red fluorescence. However, when mitochondria are damaged, Mt$\Delta\psi$ decreases, causing JC-1 to exist in monomeric form and emit green fluorescence. Consequently, the ratio of red fluorescence to green fluorescence is proportional to the Mt$\Delta\psi$. Flow cytometry and fluorescence microscope revealed that GNA treatment significantly decreased the Mt$\Delta\psi$ in 143B cells ($p < 0.05$, Fig. 3A). Moreover, 24 hours after GNA treatment, the expression of Cytochrome c in the cytoplasm and the whole cell BCL2-associated X protein (Bax) was significantly increased ($p < 0.05$), while the whole cell Apoptosis regulator Bcl-2 (Bcl-2) was substantially decreased ($p < 0.05$, Fig. 3B). These findings suggest the involvement of mitochondrial pathways in GNA-induced apoptosis within 143B cells.

GNA-Induced Autophagy in 143B Cells

Following transfection of the cells with Ad-GFP-LC3B, during non-autophagic conditions, the green fluorescence dispersed in the cytoplasm, while aggregated on the autophagosome membrane during autophagic conditions, appearing as green fluorescence puncta. As depicted in Fig. 4A, in the GNA treatment groups, numerous green spots were observed in 143B cells following 12 hours of

Journal of
BIOLOGICAL REGULATORS
and Homeostatic Agents

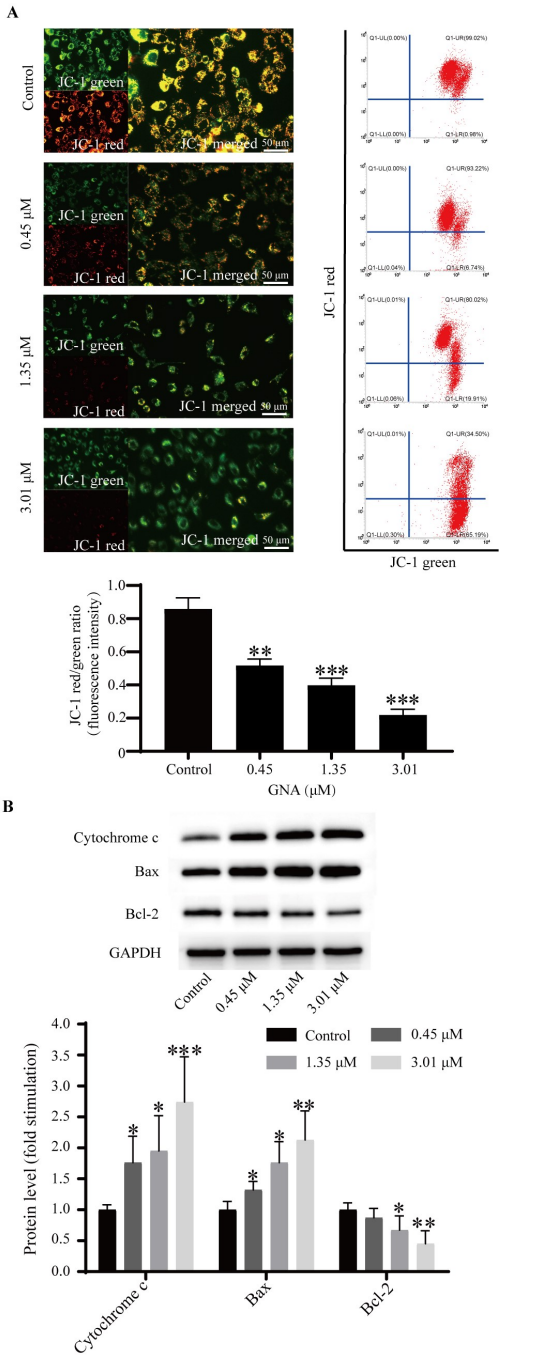

Fig. 3. GNA-induced apoptosis involves the mitochondrial pathway in 143 cells. (A) Cells stained with a 5,5′,6,6′-tetrachloro-1,1′,3,3′-tetramethylbenzimidazolylcarbocyanine iodide (JC-1) fluorescent probe were examined using a fluorescence microscope and flow cytometry. (B) Whole-cell protein was extracted to analyze Bax and Bcl-2 using Western blot, while cytosol fractions were utilized for Cytochrome c assay. $^{*}p < 0.05$ vs. the control group (n = 3), $^{**}p < 0.01$ vs. the control group (n = 3), $^{***}p < 0.001$ vs. the control group (n = 3).

treatment. However, there were no such spots found in the control group, suggesting that GNA treatment induced the formation of autophagosomes. When autophagy is initiated, microtubule-associated protein 1 light chain 3 (LC3) undergoes modification from form I to form II, which facilitates autophagosome formation. Consequently, the ratio of LC3-II/LC3-I shows the extent of autophagy [21]. Furthermore, Beclin-1 is another marker associated with the initiation of autophagy [22]. However, the autophagy receptor protein P62 undergoes degradation with the completion of the autophagy process. Western blot revealed that the levels of LC3-II/LC3-I and Beclin-1 were increased while P62 decreased following GNA treatment ($p < 0.05$, Fig. 4B). These findings suggest that GNA treatment induced autophagy in 143B cells.

GNA-Induced Autophagy can be Regulated by the ROS-JNK Signaling Pathway

The JNK pathway has been identified as crucial in regulating autophagy, with ROS that can activate c-Jun N-terminal kinase (JNK) and trigger autophagy [23–25]. We found that GNA treatment significantly increased the level of ROS and phosphorylated JNK in 143B cells ($p < 0.05$, Fig. 5A,B). We observed that NAC reversed the phosphorylation of JNK and the increased the ratio of LC3-II/LC3-I ($p < 0.05$, Fig. 5C), suggesting that the ROS induced autophagy as well as activated JNK. Furthermore, in cells pretreated with SP600125, the inhibition of JNK was accompanied by a reversal of the upregulated LC3-II/LC3-I ratio induced by GNA ($p < 0.05$, Fig. 5D). These findings suggest that GNA-induced autophagy in 143B cells can be regulated by the ROS-JNK signaling pathway.

Autophagy Induced in 143B Cells by GNA Exhibits a Protective Role against Apoptosis

The role of autophagy is intricate and differs depending on the characteristics of cells and the stimulus type. To evaluate the effect of autophagy elicited by GNA in 143B cells, we pretreated certain cells with small interfering RNA targeting *ATG5* (si*ATG5*), which hindered the autophagy process [26,27], and then subjected them to GNA treatment. Apoptosis levels were assessed employing flow cytometry. It was found that inhibition of autophagy significantly increased the GNA-induced apoptosis ($p < 0.05$, Fig. 6A,B). Furthermore, Western blot showed that inhibition of autophagy significantly decreased LC3 II expression while increasing the levels of cleaved caspase-3 and cleaved PARP ($p < 0.05$, Fig. 6C). Moreover, the CCK-8 assay revealed that autophagy inhibition enhanced the inhibitory impact of GNA on 143B cells ($p < 0.05$, Fig. 6D). These outcomes demonstrate that autophagy induced in 143B cells by GNA exhibits a protective role against apoptosis.

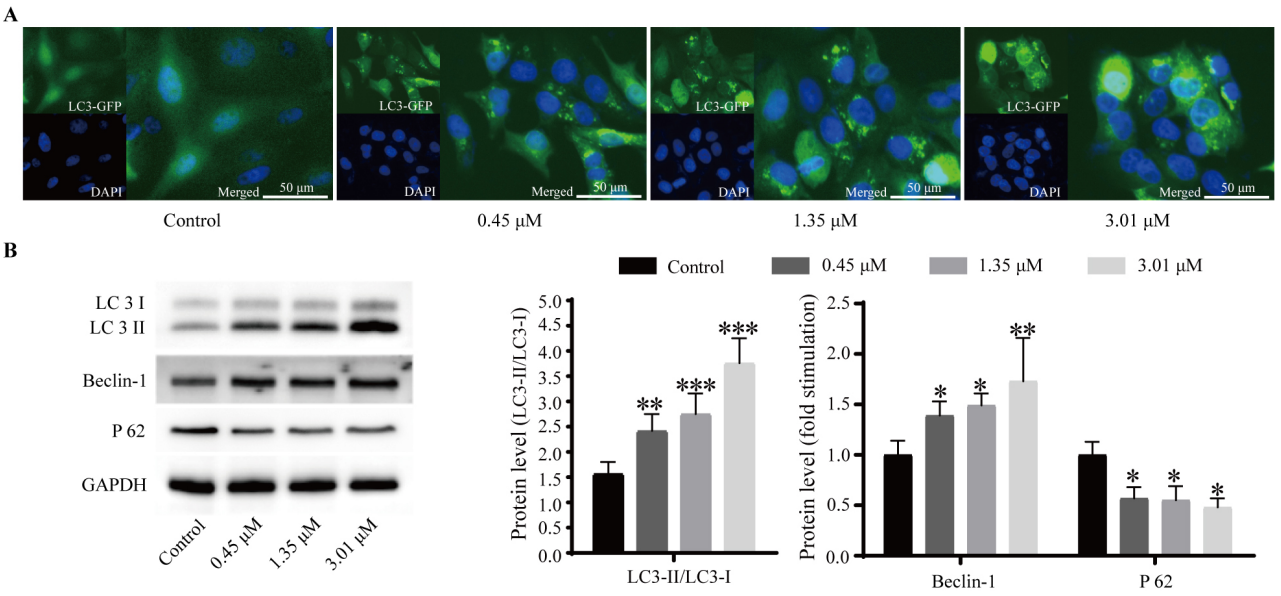

Fig. 4. GNA treatment induced autophagy of 143B cells. (A) Cells transfected with Ad-GFP-LC3B were observed using a fluorescence microscope for the formation of autophagosomes. (B) Protein expression levels were assessed through Western blot. $^{*}p < 0.05$ vs. the control group (n = 3), $^{**}p < 0.01$ vs. the control group (n = 3), $^{***}p < 0.001$ vs. the control group (n = 3).

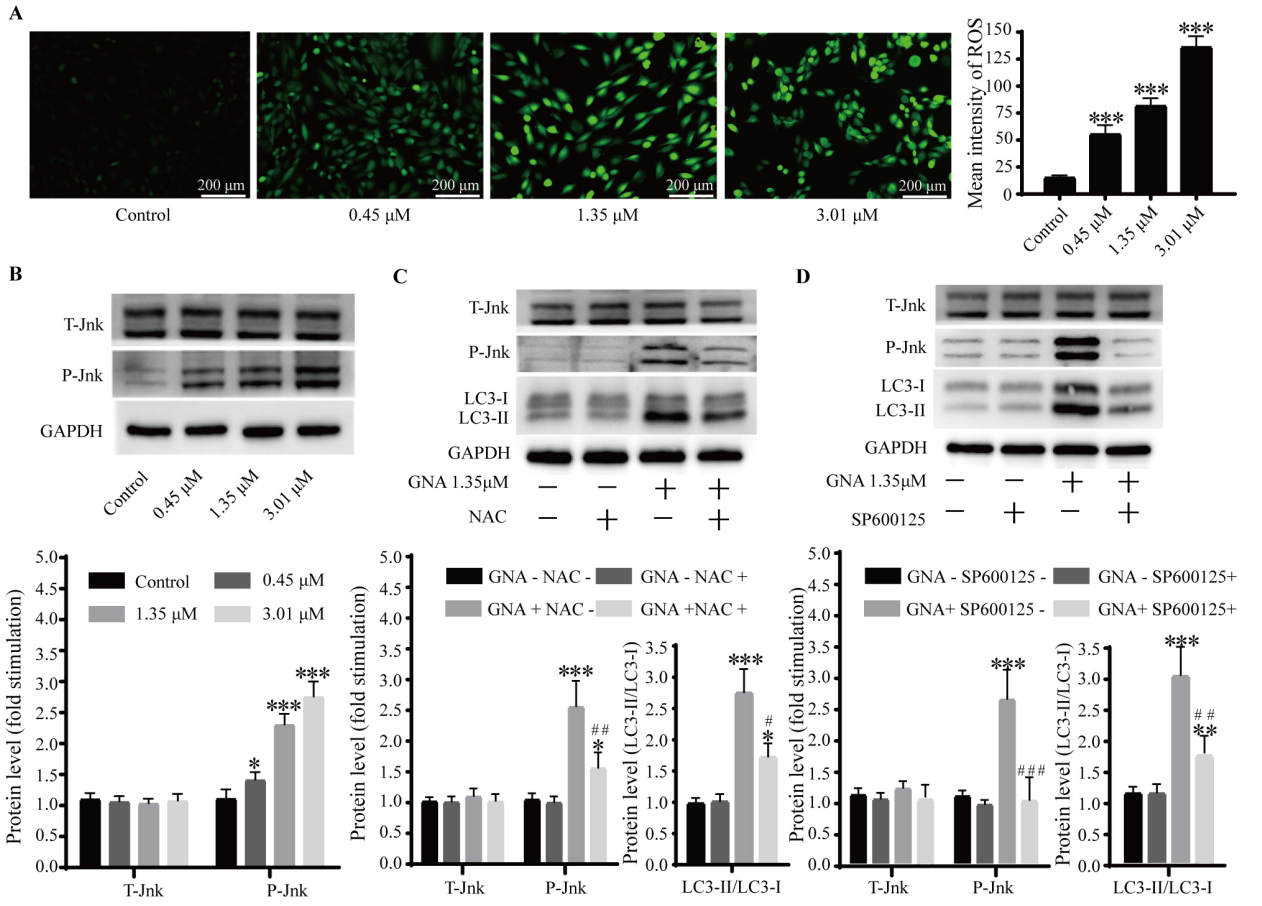

Fig. 5. GNA-induced autophagy in 143B cells can be regulated by the ROS-JNK signaling pathway. (A) ROS levels in 143B cells. (B–D) Protein expression levels were assessed through Western blot. $^{*}p < 0.05$ vs. the control group (n = 3), $^{**}p < 0.01$ vs. the control group (n = 3), $^{***}p < 0.001$ vs. the control group (n = 3), $^{\#}p < 0.05$ vs. the GNA group (n = 3), $^{\#\#}p < 0.01$ vs. the GNA group (n = 3), $^{\#\#\#}p < 0.001$ vs. the GNA group (n = 3). ROS, reactive oxygen species; NAC, N-acetyl-l-cysteine.

Journal of
BIOLOGICAL REGULATORS
and Homeostatic Agents

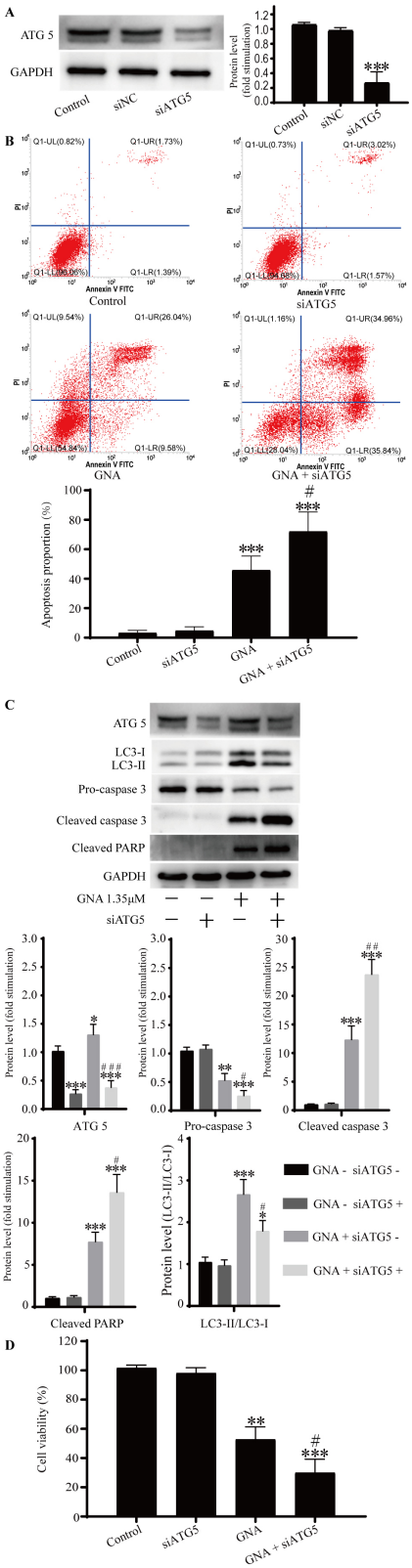

Fig. 6. Autophagy induced in 143B cells by GNA exhibits a protective role against apoptosis. (A) Knockdown efficiency of siATG5 was determined using Western blot. (B) The apoptosis rate was observed using flow cytometric analysis. (C) Protein expression levels were assessed through Western blot. (D) Cell viability. $^{*}p < 0.05$ vs. the control group (n = 3), $^{**}p < 0.01$ vs. the control group (n = 3), $^{***}p < 0.001$ vs. the control group (n = 3), $^{\#}p < 0.05$ vs. the GNA group (n = 3), $^{\#\#}p < 0.01$ vs. the GNA group (n = 3), $^{\#\#\#}p < 0.001$ vs. the GNA group (n = 3). si*ATG5*, small interfering RNA targeting *ATG5*; siNC, small interfering RNA targeting negative control.

Discussion

The standard approach for treating OS involves neoadjuvant chemotherapy combined with limb salvage surgery, contributing to a modest improvement in the survival rate of patients. Nevertheless, certain individuals may exhibit insensitivity or resistance to chemotherapy. Hence, there is a pressing need to develop novel or enhanced treatment options for OS. Chinese Medicine (CM), known for its ability to target multiple aspects and have diverse biological effects, has shown promising outcomes in treating tumors with minimal adverse reactions [28–31]. Presently, research has been focusing on the application of CMs for treating OS and has emerged as a popular area of investigation. GNA, the major bioactive component extracted from Gamboge, has been recognized for its anti-cancer properties against various tumors including OS [19]. However, the precise mechanism of GNA against OS is yet to be fully understood. Therefore, we explored the inhibitory effect and potential mechanisms of GNA in human osteosarcoma cells (143B).

The findings of our study demonstrated that GNA exhibited an inhibitory effect on 143B cells, consistent with the outcome reported by Liu *et al*. [17]. Furthermore, we investigated the potential mechanisms underlying GNA's anti-OS properties and discovered that it triggered apoptosis and autophagy in 143B cells. These two crucial cellular processes can be triggered by various treatments such as chemotherapy, radiotherapy, and other therapeutic methods [32–34]. The detailed mechanisms underlying their induction are complex and vary depending on the type of stimulus and the cellular genotype. Therefore, elucidating these mechanisms can help in regulating apoptosis and autophagy, thereby enhancing the anti-OS properties of GNA [35].

Liu *et al*. [17] reported that GNA can damage the mitochondria of OS cells, but it remains unclear whether this is related to the induction of apoptosis. The activation of the mitochondrial-related apoptotic pathway results in reduced Mt$\Delta\psi$, thereby releasing Cytochrome c from the mitochondria. Subsequently, the release of Cytochrome c, along with Apaf-1 and procaspase-9, forms a protein complex. This complex activates caspase-9, which then activates caspase-3, ultimately completing the apoptosis process [36,37]. Furthermore, the Bcl-2 group also plays a role in this process by regulating the release of Cytochrome c. Bcl-2 maintains the stability of the mitochondrial membrane permeability. Conversely, Bax can enhance membrane permeability [38–40]. These proteins serve as indicators linked to mitochondria-related apoptosis. In this research, we examined the initiation of the apoptotic pathway related to mitochondria in GNA-treated 143B cells. Our findings indicate a substantial reduction in the Mt$\Delta\psi$ of 143B cells following GNA treatment, as evidenced by the results obtained from JC-1 staining. Moreover, Western blot demonstrated that GNA triggered the release of Cytochrome c, reduced the expression of Bcl-2, and enhanced the expression of Bax in 143B cells. These findings, collectively, suggest the involvement of mitochondrial-related apoptotic pathways in GNA-induced apoptosis in 143B cells.

ROS and JNK can participate in the induction of autophagy, with ROS also serving as an activation signal for the JNK signaling pathway [41–43]. In this study, after GNA treatment, we found a significant increase in intracellular ROS levels and JNK phosphorylation. The induction of autophagy by GNA was significantly suppressed by SP600125, an inhibitor of JNK. Additionally, we discovered that NAC exhibited a substantial impact on reducing JNK phosphorylation and autophagy, indicating that ROS acts as an activator of JNK signaling. Thus, GNA-induced autophagy in 143B cells was found to be regulated by the ROS-JNK signaling pathway, as evidenced by these findings.

Furthermore, we demonstrated that GNA triggered apoptosis and autophagy in 143B cells; however, the correlation between these two processes remained uncertain. Understanding the connection between autophagy and apoptosis triggered by GNA could aid in controlling these processes, thereby enhancing the anti-cancer properties of GNA. Autophagy is a frequently used mechanism of treatment tolerance. However, Mei *et al*. [44] discovered that GNA can trigger abnormal autophagy leading to the death of lung cancer cells, and inhibition of autophagy significantly reduced the cell death caused by GNA, indicating a pro-death function of autophagy in cancer cells treated with GNA. In our study, *ATG5* gene silencing significantly magnified the level of apoptosis induced by GNA. Additionally, the CCK-8 assay revealed that *ATG5* gene silencing significantly enhanced the inhibitory effect of GNA on the viability of 143B cells. Therefore, inhibiting autophagy may be a method to enhance the anti-osteosarcoma effects of GNA.

Conclusions

In conclusion, GNA induced apoptosis and autophagy in 143B cells, with apoptosis being associated with the mitochondrial pathway and autophagy being regulated by the ROS-JNK signaling pathway. Furthermore, autophagy played a cell-protective role against apoptosis.

Availability of Data and Materials

All experimental data included in this study can be obtained by contacting the corresponding author if needed.

Author Contributions

RZ, TL and XL designed the research study. RZ and TL performed the research. PQ, XW, BQ and XS provided help on the cell culture, Western blot and siRNA trasfec-

Journal of
BIOLOGICAL REGULATORS
and Homeostatic Agents

tion experiments and statistical analysis. All authors contributed to editorial changes in the manuscript. All authors read and approved the final manuscript. All authors have participated sufficiently in the work and agreed to be accountable for all aspects of the work.

Ethics Approval and Consent to Participate

Not applicable.

Acknowledgment

Not applicable.

Funding

This research received no external funding.

Conflict of Interest

The authors declare no conflict of interest.

References

[1] Gill J, Gorlick R. Advancing therapy for osteosarcoma. Nature Reviews. Clinical Oncology. 2021; 18: 609–624.
[2] Belayneh R, Fourman MS, Bhogal S, Weiss KR. Update on Osteosarcoma. Current Oncology Reports. 2021; 23: 71.
[3] Benjamin RS. Adjuvant and Neoadjuvant Chemotherapy for Osteosarcoma: A Historical Perspective. Advances in Experimental Medicine and Biology. 2020; 1257: 1–10.
[4] Sugito W, Kamal AF. Clinical Outcome Following Prolonged Neoadjuvant Chemotherapy and Delayed Surgery in Osteosarcoma Patients: An Evidence-based Clinical Review. Acta Medica Indonesiana. 2022; 54: 142–150.
[5] Khadembaschi D, Jafri M, Praveen P, Parmar S, Breik O. Does neoadjuvant chemotherapy provide a survival benefit in maxillofacial osteosarcoma: A systematic review and pooled analysis. Oral Oncology. 2022; 135: 106133.
[6] Zhu W, Zhu L, Bao Y, Zhong X, Chen Y, Wu Q. Clinical evaluation of neoadjuvant chemotherapy for osteosarcoma. Journal of B.U.ON. 2019; 24: 1181–1185.
[7] Smeland S, Bielack SS, Whelan J, Bernstein M, Hogendoorn P, Krailo MD, *et al*. Survival and prognosis with osteosarcoma: outcomes in more than 2000 patients in the EURAMOS-1 (European and American Osteosarcoma Study) cohort. European Journal of Cancer. 2019; 109: 36–50.
[8] Da W, Tao Z, Meng Y, Wen K, Zhou S, Yang K, *et al*. A 10-year bibliometric analysis of osteosarcoma and cure from 2010 to 2019. BMC Cancer. 2021; 21: 115.
[9] Wang B, Yuan T, Zha L, Liu Y, Chen W, Zhang C, *et al*. Oral Delivery of Gambogenic Acid by Functional Polydopamine Nanoparticles for Targeted Tumor Therapy. Molecular Pharmaceutics. 2021; 18: 1470–1479.
[10] Wang M, Li S, Wang Y, Cheng H, Su J, Li Q. Gambogenic acid induces ferroptosis in melanoma cells undergoing epithelial-to-mesenchymal transition. Toxicology and Applied Pharmacology. 2020; 401: 115110.
[11] Zhou S, Zhao N, Wang J. Gambogenic acid suppresses bladder cancer cells growth and metastasis by regulating NF-κB signaling. Chemical Biology & Drug Design. 2020; 96: 1272–1279.
[12] Liu C, Xu J, Guo C, Chen X, Qian C, Zhang X, *et al*. Gambogenic Acid Induces Endoplasmic Reticulum Stress in Colorectal Cancer via the Aurora A Pathway. Frontiers in Cell and Developmental Biology. 2021; 9: 736350.
[13] Yan F, Wang M, Chen H, Su J, Wang X, Wang F, *et al*. Gambogenic acid mediated apoptosis through the mitochondrial oxidative stress and inactivation of Akt signaling pathway in human nasopharyngeal carcinoma CNE-1 cells. European Journal of Pharmacology. 2011; 652: 23–32.
[14] Rakesh R, PriyaDharshini LC, Sakthivel KM, Rasmi RR. Role and regulation of autophagy in cancer. Biochimica et Biophysica Acta. Molecular Basis of Disease. 2022; 1868: 166400.
[15] Ravikumar B, Sarkar S, Davies JE, Futter M, Garcia-Arencibia M, Green-Thompson ZW, *et al*. Regulation of mammalian autophagy in physiology and pathophysiology. Physiological Reviews. 2010; 90: 1383–1435.
[16] Chen X, Zhang X, Cai H, Yang W, Lei H, Xu H, *et al*. Targeting USP9x/SOX2 axis contributes to the anti-osteosarcoma effect of neogambogic acid. Cancer Letters. 2020; 469: 277–286.
[17] Liu Z, Wang X, Li J, Yang X, Huang J, Ji C, *et al*. Gambogenic acid induces cell death in human osteosarcoma through altering iron metabolism, disturbing the redox balance, and activating the P53 signaling pathway. Chemico-Biological Interactions. 2023; 382: 110602.
[18] Wang M, Zhan F, Cheng H, Li Q. Gambogenic Acid Inhibits Basal Autophagy of Drug-Resistant Hepatoma Cells and Improves Its Sensitivity to Adriamycin. Biological & Pharmaceutical Bulletin. 2022; 45: 63–70.
[19] Wu J, Wang D, Zhou J, Li J, Xie R, Li Y, *et al*. Gambogenic acid induces apoptosis and autophagy through ROS-mediated endoplasmic reticulum stress via JNK pathway in prostate cancer cells. Phytotherapy Research. 2023; 37: 310–328.
[20] Bock FJ, Tait SWG. Mitochondria as multifaceted regulators of cell death. Nature Reviews. Molecular Cell Biology. 2020; 21: 85–100.
[21] Jeong YH, Kim TI, Oh YC, Ma JY. *Selaginella tamariscina* Inhibits Glutamate-Induced Autophagic Cell Death by Activating the PI3K/AKT/mTOR Signaling Pathways. International Journal of Molecular Sciences. 2022; 23: 11445.
[22] Kopiasz Ł, Dziendzikowska K, Oczkowski M, Harasym J, Gromadzka-Ostrowska J. Low-molar-mass oat beta-glucan impacts autophagy and apoptosis in early stages of induced colorectal carcinogenesis in rats. International Journal of Biological Macromolecules. 2024; 254: 127832.
[23] Li X, Wang Y, Chen Y, Zhou P, Wei K, Wang H, *et al*. Hierarchically constructed selenium-doped bone-mimetic nanoparticles promote ROS-mediated autophagy and apoptosis for bone tumor inhibition. Biomaterials. 2020; 257: 120253.
[24] Liu X, Zhao P, Wang X, Wang L, Zhu Y, Song Y, *et al*. Celastrol mediates autophagy and apoptosis via the ROS/JNK and Akt/mTOR signaling pathways in glioma cells [published correction appears in Journal of Experimental & Clinical Cancer Research. 2019; 38: 284]. Journal of Experimental & Clinical Cancer Research. 2019; 38: 184.
[25] Chan CM, Huang DY, Sekar P, Hsu SH, Lin WW. Reactive oxygen species-dependent mitochondrial dynamics and autophagy confer protective effects in retinal pigment epithelial cells against sodium iodate-induced cell death [published correction appears in Journal of Biomedical Science. 2019; 26: 66]. Journal of Biomedical Science. 2019; 26: 40.
[26] Zhou P, Li Y, Li B, Zhang M, Xu C, Liu F, *et al*. Autophagy inhibition enhances celecoxib-induced apoptosis in osteosarcoma. Cell Cycle. 2018; 17: 997–1006.
[27] Huang Y, Liu W, He B, Wang L, Zhang F, Shu H, *et al*. Exosomes derived from bone marrow mesenchymal stem cells promote osteosarcoma development by activating oncogenic autophagy. Journal of Bone Oncology. 2020; 21: 100280.
[28] Yin MC, Wang HS, Yang X, Xu CQ, Wang T, Yan YJ, *et al*.

A Bibliometric Analysis and Visualization of Current Research Trends in Chinese Medicine for Osteosarcoma. Chinese Journal of Integrative Medicine. 2022; 28: 445–452.

[29] Liang D, Liu L, Zheng Q, Zhao M, Zhang G, Tang S, *et al*. Chelerythrine chloride inhibits the progression of colorectal cancer by targeting cancer-associated fibroblasts through intervention with WNT10B/β-catenin and TGFβ2/Smad2/3 axis. Phytotherapy Research. 2023; 37: 4674–4689.

[30] Yu J, Wang J, Yang J, Ouyang T, Gao H, Kan H, *et al*. New insight into the mechanisms of Ginkgo biloba leaves in the treatment of cancer. Phytomedicine. 2024; 122: 155088.

[31] Kazantseva L, Becerra J, Santos-Ruiz L. Traditional Medicinal Plants as a Source of Inspiration for Osteosarcoma Therapy. Molecules. 2022; 27: 5008.

[32] Zhang Y, Huang Q, Xu Q, Jia C, Xia Y. Pimavanserin tartrate induces apoptosis and cytoprotective autophagy and synergizes with chemotherapy on triple negative breast cancer. Biomedicine & Pharmacotherapy. 2023; 168: 115665.

[33] Yang W, Cheng B, Chen P, Sun X, Wen Z, Cheng Y. BTN3A1 promotes tumor progression and radiation resistance in esophageal squamous cell carcinoma by regulating ULK1-mediated autophagy. Cell Death & Disease. 2022; 13: 984.

[34] Chien LH, Deng JS, Jiang WP, Chou YN, Lin JG, Huang GJ. Evaluation of lung protection of Sanghuangporus sanghuang through TLR4/NF-κB/MAPK, keap1/Nrf2/HO-1, CaMKK/AMPK/Sirt1, and TGF-β/SMAD3 signaling pathways mediating apoptosis and autophagy. Biomedicine & Pharmacotherapy. 2023; 165: 115080.

[35] Almansa-Gómez S, Prieto-Ruiz F, Cansado J, Madrid M. Autophagy Modulation as a Potential Therapeutic Strategy in Osteosarcoma: Current Insights and Future Perspectives. International Journal of Molecular Sciences. 2023; 24: 13827.

[36] Li Z, Guo D, Yin X, Ding S, Shen M, Zhang R, *et al*. Zinc oxide nanoparticles induce human multiple myeloma cell death via reactive oxygen species and Cyt-C/Apaf-1/Caspase-9/Caspase-3 signaling pathway in vitro. Biomedicine & Pharmacotherapy. 2020; 122: 109712.

[37] Jemmerson R, Staskus K, Higgins L, Conklin K, Kelekar A. Intracellular leucine-rich alpha-2-glycoprotein-1 competes with Apaf-1 for binding cytochrome c in protecting MCF-7 breast cancer cells from apoptosis. Apoptosis. 2021; 26: 71–82.

[38] Hauseman ZJ, Harvey EP, Newman CE, Wales TE, Bucci JC, Mintseris J, *et al*. Homogeneous Oligomers of Pro-apoptotic BAX Reveal Structural Determinants of Mitochondrial Membrane Permeabilization. Molecular Cell. 2020; 79: 68–83.e7.

[39] Dadsena S, Jenner A, García-Sáez AJ. Mitochondrial outer membrane permeabilization at the single molecule level. Cellular and Molecular Life Sciences. 2021; 78: 3777–3790.

[40] Shalaby R, Flores-Romero H, García-Sáez AJ. The Mysteries around the BCL-2 Family Member BOK. Biomolecules. 2020; 10: 1638.

[41] Pajares M, Cuadrado A, Engedal N, Jirsova Z, Cahova M. The Role of Free Radicals in Autophagy Regulation: Implications for Ageing. Oxidative Medicine and Cellular Longevity. 2018; 2018: 2450748.

[42] Deng Y, Adam V, Nepovimova E, Heger Z, Valko M, Wu Q, *et al*. c-Jun N-terminal kinase signaling in cellular senescence. Archives of Toxicology. 2023; 97: 2089–2109.

[43] Zhong L, Shu W, Dai W, Gao B, Xiong S. Reactive Oxygen Species-Mediated c-Jun NH_2-Terminal Kinase Activation Contributes to Hepatitis B Virus X Protein-Induced Autophagy via Regulation of the Beclin-1/Bcl-2 Interaction. Journal of Virology. 2017; 91: e00001-17.

[44] Mei W, Dong C, Hui C, Bin L, Fenggen Y, Jingjing S, *et al*. Gambogenic acid kills lung cancer cells through aberrant autophagy. PLoS ONE. 2014; 9: e83604.